Available online at www.eccomasproceedia.org
Eccomas Proceedia COMPDYN (2017) 2719-2728

ECCOMAS
Proceedia

COMPDYN 2017
6th ECCOMAS Thematic Conference on
Computational Methods in Structural Dynamics and Earthquake Engineering
M. Papadrakakis, M. Fragiadakis (eds.)
Rhodes Island, Greece, 15–17 June, 2017

SYNCHRONIZATION OF DATA ACQUISITION SYSTEMS FOR THE PURPOSE OF STRUCTURAL HEALTH MONITORING

K. Maes[1], E. Reynders[1], A. Rezayat[2], G. De Roeck[1], and G. Lombaert[1]

[1]KU Leuven, Department of Civil Engineering
Kasteelpark Arenberg 40, 3001 Leuven, Belgium
e-mail: kristof.maes@kuleuven.be

[2] Vrije Universiteit Brussel, Department of Mechanical Engineering
Pleinlaan 2, 1050 Brussels, Belgium
e-mail: arezayat@vub.ac.be

Keywords: Time synchronization, data acquisition, system identification, output-only, structural health monitoring

Abstract. *This paper presents a technique for offline time synchronization of data acquisition systems for linear structures with proportional damping. The technique can be applied when direct synchronization of data acquisition systems is impossible or not sufficiently accurate, for example when multiple measurement nodes with different clock signals are embedded in a health monitoring network. The synchronization is based on the acquired dynamic response of the structure only, and does not require the acquisition of a shared sensor signal or a trigger signal. The time delay is identified from the spurious phase shift of the mode shape components that are obtained from system identification. A demonstration for a laboratory experiment on a cantilever steel beam shows that the proposed methodology can be used for accurate time synchronization, resulting in a significant improvement of the accuracy of the identified mode shapes.*

Peer-review under responsibility of the organizing committee of COMPDYN 2017.
doi: 10.7712/120117.5601.17604

1 INTRODUCTION

Structural health monitoring often requires the use of multiple data acquisition systems, due to the large number of measurement channels, the large distance between sensors, or the need for heterogeneous sensor data. This creates the need for synchronization of data acquisition systems. Currently, monitoring systems consisting of multiple wireless nodes are being developed [2, 10]. Each of the nodes has its own data acquisition, and–to date–synchronization of the nodes remains a challenge. Several techniques for (online) synchronization of measurement systems have been proposed so far, amongst which time stamping through GPS [5], and synchronization through fiber optical cables or radio communication.

When direct time synchronization of data acquisition systems is impossible or insufficiently accurate, offline synchronization of recorded vibration data is needed. When a sensor signal is shared by multiple data acquisition systems, offline synchronization can be easily performed by applying correlation techniques or by calculating the transfer function that relates both measured signals [1]. This is not always possible, for example when a network of independent wireless sensors at different locations on the structure is used. This paper presents a technique that enables for offline time synchronization of data acquisition systems. The technique assumes linear time-invariant dynamic behavior of the structure and proportional damping of the structural modes. The synchronization time delay is identified from the spurious phase shift of the mode shape components, that are obtained from system identification.

The paper is outlined as follows. Section 2 shows that a synchronization time lag results in a phase shift of the identified mode shapes, whereas the identified natural frequencies and modal damping ratios are unchanged. Next, section 3 demonstrates using data obtained from a laboratory experiment on a cantilever beam how the findings in section 2 can be applied for offline synchronization of data acquisition systems. Finally, in section 4, the work is concluded.

2 MATHEMATICAL BACKGROUND

Consider two response signals $d_1(t)$ and $d_2(t)$ obtained from sensors installed at arbitrary locations on the structure. The signals may correspond to different response quantities, e.g. acceleration or strain. Under the assumption of linear system behavior, the Laplace transform of the response signals, $d_1(s) \in \mathbb{C}$ and $d_2(s) \in \mathbb{C}$, are related through the transmissibility function $T(s) \in \mathbb{C}$ as follows [11]:

$$d_1(s) = T(s)d_2(s) \tag{1}$$

where $s \in \mathbb{C}$ is the Laplace variable [12]. Furthermore, the Laplace transform of the response signals $d_1(s)$ and $d_2(s)$ is related to the Laplace transform of the load vector $\mathbf{p}(s) \in \mathbb{C}^{n_\mathrm{p}}$ through the transfer function matrices $\mathbf{H}_1(s) \in \mathbb{C}^{1\times n_\mathrm{p}}$ and $\mathbf{H}_2(s) \in \mathbb{C}^{1\times n_\mathrm{p}}$, respectively, as given by the following equation:

$$d_1(s) = \mathbf{H}_1(s)\mathbf{p}(s) \tag{2}$$

$$d_2(s) = \mathbf{H}_2(s)\mathbf{p}(s) \tag{3}$$

It assumed here that n_p loads are acting on the structure. The number of loads and their location is not important for the derivation following next, however. Under the assumption that the response of the structure within a certain frequency range of interest is well approximated by a limited number of structural modes (n_m modes), and assuming in addition proportional

damping, the transfer function matrices $\mathbf{H}_1(s)$ and $\mathbf{H}_2(s)$ are given by:

$$\mathbf{H}_1(s) = \sum_{m=1}^{n_\mathrm{m}} \frac{s^{q_1}\phi_{\mathrm{d}_1 m}}{s^2 + 2\xi_m\omega_m s + \omega_m^2}\boldsymbol{\phi}_{\mathrm{p}m} = \sum_{m=1}^{n_\mathrm{m}} s^{q_1}\phi_{\mathrm{d}_1 m}\mathbf{H}'_m(s) \tag{4}$$

$$\mathbf{H}_2(s) = \sum_{m=1}^{n_\mathrm{m}} \frac{s^{q_2}\phi_{\mathrm{d}_2 m}}{s^2 + 2\xi_m\omega_m s + \omega_m^2}\boldsymbol{\phi}_{\mathrm{p}m} = \sum_{m=1}^{n_\mathrm{m}} s^{q_2}\phi_{\mathrm{d}_2 m}\mathbf{H}'_m(s) \tag{5}$$

where $\mathbf{H}'_m(s) = \boldsymbol{\phi}_{\mathrm{p}m}/(s^2 + 2\xi_m\omega_m s + \omega_m^2)$, with $\boldsymbol{\phi}_{\mathrm{p}m} \in \mathbb{R}^{1\times n_\mathrm{p}}$ the vector of mode shape components corresponding to mode m at the n_p force locations. ω_m and ξ_m are the undamped natural frequency and the modal damping ratio of mode m, respectively. $\phi_{\mathrm{d}_1 m}$ and $\phi_{\mathrm{d}_2 m}$ are obtained by selecting the component of the mode shape vector corresponding to mode m at the sensor locations of d_1 and d_2, respectively. The integers q_1 and q_2 equal 0 for displacement or strain measurements, 1 for velocity measurements, and 2 for acceleration measurements.

The system has $2n_\mathrm{m}$ poles, occurring in complex conjugate pairs, λ_{m1} and λ_{m2} ($m = 1, \ldots, n_\mathrm{m}$), given by the following expression [6]:

$$\lambda_{m1,2} = -\omega_m\xi_m \pm i\omega_m\sqrt{1-\xi_m^2} \tag{6}$$

where $i = \sqrt{-1}$. The poles λ_{m1} and λ_{m2} correspond to the natural frequency ω_m and modal damping ratio ξ_m of mode m. When the transfer function matrices in Eqs. (4) and (5) are evaluated at a system pole, i.e. $s = \lambda_{m1}$, only the corresponding mode m contributes to the system response [4], and the following expressions are obtained:

$$\mathbf{H}_1(\lambda_{m1}) = \lambda_{m1}^{q_1}\phi_{\mathrm{d}_1 m}\mathbf{H}'_m(\lambda_{m1}) \tag{7}$$

$$\mathbf{H}_2(\lambda_{m1}) = \lambda_{m1}^{q_2}\phi_{\mathrm{d}_2 m}\mathbf{H}'_m(\lambda_{m1}) \tag{8}$$

Combination of Eqs. (7) and (8) directly yields:

$$\mathbf{H}_1(\lambda_{m1}) = \frac{\lambda_{m1}^{q_1}\phi_{\mathrm{d}_1 m}}{\lambda_{m1}^{q_2}\phi_{\mathrm{d}_2 m}}\mathbf{H}_2(\lambda_{m1}) \tag{9}$$

Evaluation of Eqs. (2) and (3) at the system pole $s = \lambda_{m1}$, and taking into account Eq. (9) yields:

$$d_1(\lambda_{m1}) = \frac{\lambda_{m1}^{q_1}\phi_{\mathrm{d}_1 m}}{\lambda_{m1}^{q_2}\phi_{\mathrm{d}_2 m}}d_2(\lambda_{m1}) \tag{10}$$

such that

$$T(\lambda_{m1}) = \frac{\lambda_{m1}^{q_1}\phi_{\mathrm{d}_1 m}}{\lambda_{m1}^{q_2}\phi_{\mathrm{d}_2 m}} \tag{11}$$

Next, consider the response signal $d'_2(t)$, that is obtained by applying a time delay δt to the response signal $d_2(t)$, i.e. $d'_2(t) = d_2(t-\delta t)$. The Laplace transforms of the response signals $d_1(t)$ and $d'_2(t)$ are related through the transmissibility function $T'(s)$, i.e. $d_1(s) = T'(s)d'_2(s)$. The transmissibility function $T'(s)$ is related to the transmissibility function $T(s)$ as follows [12]:

$$T'(s) = T(s)e^{s\delta t} \tag{12}$$

Evaluation of the transmissibility function $T'(s)$ at the system pole $s = \lambda_{m1}$ yields:

$$T'(\lambda_{m1}) = \frac{\lambda_{m1}^{q_1}\phi_{\mathrm{d}_1 m}}{\lambda_{m1}^{q_2}\phi'_{\mathrm{d}_2 m}} = \frac{\lambda_{m1}^{q_1}\phi_{\mathrm{d}_1 m}}{\lambda_{m1}^{q_2}\phi_{\mathrm{d}_2 m}e^{-\lambda_{m1}\delta t}} \tag{13}$$

Comparison of Eqs. (11) and (13) shows that processing the time delayed data $d'_2(t)$ together with other non-delayed data results in a (complex) mode shape component $\phi'_{\mathrm{d}_2 m}$, that is obtained from the mode shape component $\phi_{\mathrm{d}_2 m}$ by multiplication with $e^{-\lambda_{m1}\delta t}$. This corresponds to a phase shift θ_m (in radians) and a rescaling of the mode shape by the factor A_m, defined as

$$\theta_m = -\delta t\, \omega_m \sqrt{1-\xi_m^2} \tag{14}$$

$$A_m = e^{\omega_m \xi_m \delta t} \tag{15}$$

The poles of the system and, therefore, the natural frequencies and modal damping ratios, are not affected by the time delay.

For linear structures with proportional damping, the (complex) mode shape vectors $\boldsymbol{\phi}_m \in \mathbb{C}^{n_\mathrm{d}}$, containing the components $\phi_{\mathrm{d}_j m}$, can be rescaled such that real vectors are obtained. This is illustrated in Fig. 1, where a mode shape vector $\boldsymbol{\phi}_m$ is schematically represented in the complex plane, after rescaling such that the largest mode shape component becomes 1 (a.k.a. rescaling to unit modal displacement). The figure also shows the mode shape component $\phi'_{\mathrm{d}_2 m}$ as obtained from the time delayed response signal $d'_2(t)$ and using the same scaling factor. The phase angle between the mode shape components $\phi_{\mathrm{d}_2 m}$ and $\phi'_{\mathrm{d}_2 m}$ is θ_m, and is introduced by the multiplication of $\phi_{\mathrm{d}_2 m}$ with $e^{-\lambda_{m1}\delta t}$. The rescaling of the mode shape amplitude by A_m is also shown in the figure.

The phase shift of the mode shape components, introduced by the time delay δt, can be used for offline synchronization of data acquisition systems, as illustrated in Section 3.

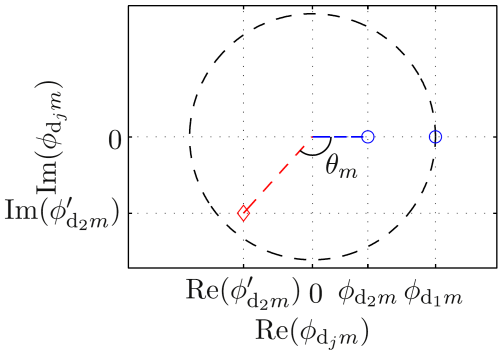

Figure 1: Representation of the mode shape components $\phi_{\mathrm{d}_1 m}$ and $\phi_{\mathrm{d}_2 m}$ (blue circles), and $\phi'_{\mathrm{d}_2 m}$ (red diamond) in the complex plane. The mode shape vector is normalized to unit modal displacement.

3 SYNCHRONIZATION APPROACH

It is demonstrated in this section how system identification techniques can be used for offline synchronization of data acquisition systems, based on the findings of Section 2. The test setup considered in the demonstration consists of a cantilever steel beam (Fig. 2a), that has been equipped with 2 uniaxial accelerometers and 22 optical fiber strain gauges (Fig. 2b). The beam has a free length of 855 mm and a rectangular cross section of 30 mm by 10 mm. The beam is clamped between two metallic plates of 200 mm by 300 mm by 20 mm each, that are bolted to a concrete support by five bolts (see Fig. 2a). The beam is clamped over a length of 120 mm. The structure is excited vertically by an inertial shaker, that has been installed underneath the beam (Fig. 2c). A load cell has been installed between the shaker and the beam to measure the applied (external) force. In addition, a small instrumented impact hammer is used for excitation. The sensor configuration is shown in Fig. 3.

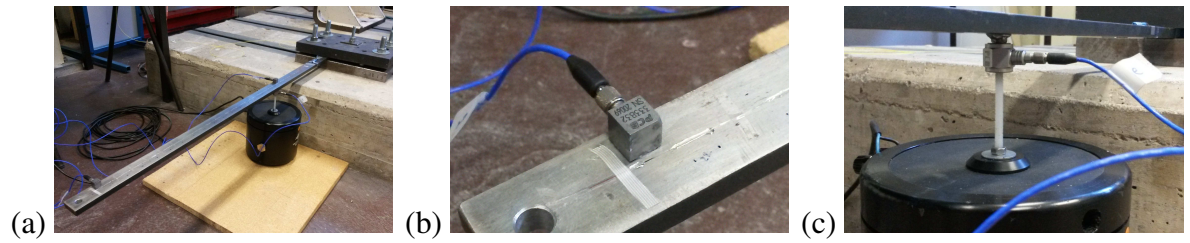

Figure 2: Overview (a) cantilever beam, (b) uniaxial accelerometer and optical fiber strain gauges, and (c) shaker and load cell.

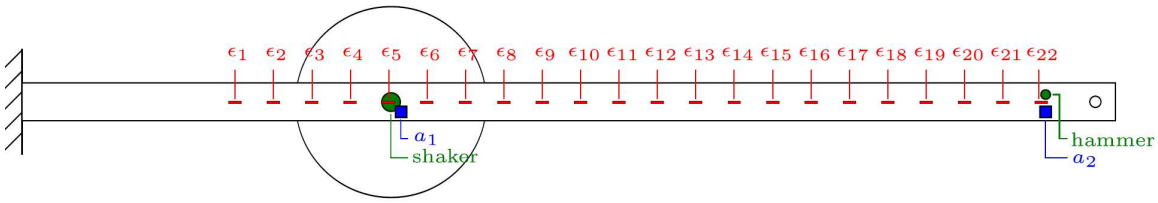

Figure 3: Sensor configuration of the laboratory experiment (a_i: accelerometer i, ϵ_i: strain gauge i).

Two data acquisition systems are used in the setup. A National Instruments (NI) data acquisition system (NI USB-6229) is used to record the data from the uniaxial accelerometers (PCB 333B32), the impact hammer (PCB 302A07) and the load cell (PCB 208B02). An FBG-Scan 700 measurement device (FBGS) has been used to record the data from the optical fiber strain gauges. A sampling frequency f_s of 1000 Hz has been used for both systems. The synchronization of the data acquisition systems is performed as follows: a trigger pulse is sent by the NI system to the FBGS system at every sampling time step. The FBGS system records a sample of the strain signals on receipt of this pulse. During the data processing, a lack of synchronization between both systems was observed. The synchronization time lag, which is in this case due to processing within the FBGS system, is determined in the following.

3.1 System identification

The modal parameters of the cantilever beam have been experimentally identified by means of an input-output system identification. The measurements for system identification were performed with vertical swept sine excitation, applied by the inertial shaker. The excitation frequency varies from 0 Hz to 500 Hz in 10 s. Fifteen sweep cycles of 10 s are considered, yielding a total measurement duration of 150 s.

The output signals used in the system identification consist of the two acceleration signals (units: $\mathrm{m/s^2}$), obtained from the NI system, and the 22 strain signals (units: $\mu\mathrm{m/m}$), obtained from the FBGS system. For all acceleration signals, the (physically meaningless) DC component is removed. The input signal consists of the shaker force signal, obtained from the NI system. The output and input signals are processed using the reference-based data-driven combined deterministic-stochastic subspace identification (CSI-data/ref) algorithm [7]. The entire record of 150 s is processed at once. No averaging or windowing is applied. The input-output modal test allows to obtain the natural frequencies, modal damping ratios, and mode shapes corresponding to the first four vertical bending modes of the cantilever beam. Table 1 presents for each of the identified modes the undamped natural frequency, the modal damping ratio, and the mode type. Fig. 4 represents the identified mode shapes in the complex plane. The amplitude of the strain mode shape components has been modified for plotting, in order to obtain

displacement and strain mode shapes with similar amplitude. After rescaling, both the displacement and strain mode shapes have a maximum amplitude of 1. The displacement mode shapes, as obtained from the acceleration data, are out of phase with the strain mode shapes. This is emphasized by plotting a line fit for the displacement and strain mode shapes separately. The angle between the fitted line and the real axis is also known as the mean phase (MP) of the mode shape, and is calculated by solving the following total least squares problem [8, 9]:

$$\mathrm{MP}(\boldsymbol{\phi}_m) = \arg\min_{\boldsymbol{\alpha}\in\mathbb{R}} \frac{||\mathrm{Im}(\boldsymbol{\phi}_m) - \tan(\alpha)\mathrm{Re}(\boldsymbol{\phi}_m)||_2^2}{1+\tan(\alpha)} \tag{16}$$

The solution is obtained as [3]:

$$\mathrm{MP}(\boldsymbol{\phi}_m) = \arctan\left(\frac{-V_{12}}{V_{22}}\right) \tag{17}$$

where V_{12} and V_{22} are the elements (1,2) and (2,2) of the matrix of right singular vectors $\mathbf{V} \in \mathbb{R}^{2\times 2}$, obtained from the singular value decomposition $\mathbf{USV}^{\mathrm{T}} = [\mathrm{Re}(\boldsymbol{\phi}_m)\ \mathrm{Im}(\boldsymbol{\phi}_m)]$, with $\mathbf{U} \in \mathbb{R}^{n_\mathrm{d}\times 2}$ and $\mathbf{S} \in \mathbb{R}^{2\times 2}$. Note that the calculation of the MP in Eq. (17) is more accurate than the classical expression for the MP provided in [4]. The latter fails when the mode shape components have an imaginary part that becomes large compared to the real part (see also [8]).

In this case, a distinction is made between the MP of the displacement mode shapes $\boldsymbol{\phi}_{am}$ and of the strain mode shapes $\boldsymbol{\phi}'_{\epsilon m}$, in order to distinguish between both measurement systems. Given that the displacement and strain mode shapes are both collinear (Fig. 4), it can be assumed that the studied system is proportionally damped, and that the difference in MP between the displacement and strain mode shapes mainly originates from the synchronization error. The time delay δt between both data acquisition systems is determined in the following section.

No.	f_id [Hz]	ξ_id [%]	Type
1	10.86	2.39	1st vertical bending mode
2	67.67	0.29	2nd vertical bending mode
3	189.37	0.28	3rd vertical bending mode
4	375.45	0.11	4th vertical bending mode

Table 1: Identified modal characteristics (f_id: undamped natural frequency, ξ_id: modal damping ratio).

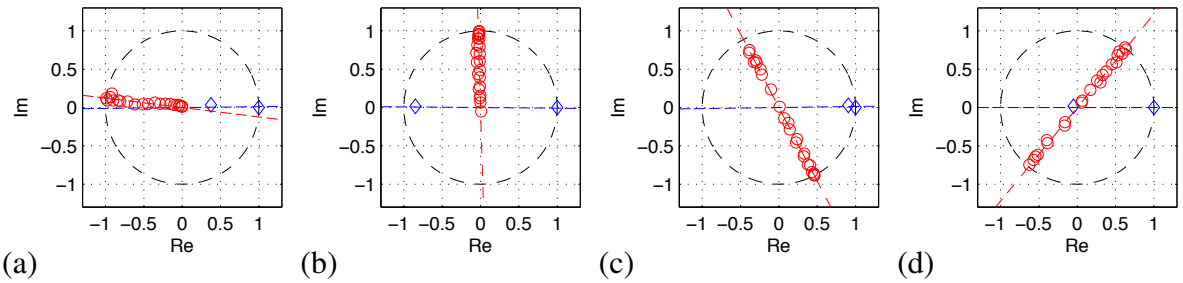

Figure 4: Representation of (a) mode 1, (b) mode 2, (c) mode 3, and (d) mode 4, in the complex plane. The displacement mode shape components obtained from the acceleration measurements are indicated by blue diamonds. The strain mode shape components are indicated by red circles. A line fit for the displacement and strain mode shape is shown by a blue and red dashed line, respectively.

3.2 Synchronization

The time delay δt is estimated by minimization of the objective function $f(\delta t)$, that gives the average difference between the MP of the displacement and the strain mode shapes over all modes. In the calculation of the objective function, the strain mode shapes $\boldsymbol{\phi}'_{\epsilon m}$ are rescaled, in order to account for a time delay δt. The displacement mode shapes $\boldsymbol{\phi}_{\mathrm{a}m}$ are not rescaled.

$$\delta t^\star = \arg\min_{\delta t \in \mathbb{R}} f(\delta t) = \arg\min_{\delta t \in \mathbb{R}} \frac{1}{n_\mathrm{m}} \sum_{m=1}^{n_\mathrm{m}} \left| \mathrm{MP}(\boldsymbol{\phi}'_{\epsilon m} e^{\lambda_{m1}\delta t}) - \mathrm{MP}(\boldsymbol{\phi}_{\mathrm{a}m}) \right| \tag{18}$$

Equal weight is given to the contribution of all modes in the objective function. For modes with a higher natural frequency, however, the phase shift θ_m introduced by a time delay δt becomes larger than for modes with a low natural frequency, as seen from Eq. (14). Modes with a higher natural frequency are therefore more sensitive to a time delay.

Figure 5 shows the objective function $f(\delta t)$ as a function the time delay δt. The objective function is not smooth and shows multiple local minima. The non smooth problem is solved by applying a sweep over all possible values of δt. The global minimum is in this case obtained for $\delta t = 3.6$ ms $(= \delta t^\star)$. The use of multiple modes is essential when estimating the time delay. If a single mode is used in the estimation, the objective function in Eq. (18) shows multiple (local) minima at $\delta t^\star \pm \pi/(\omega_m \sqrt{1-\xi_m^2})$. By including more modes, the number of minima is reduced. Since the presence of multiple optima cannot be avoided, an initial guess of the time delay is required in any case, however. This initial guess can for example be obtained by applying conventional correlation techniques. Note that the initial guess obtained from correlation techniques equals an integer number of time steps Δt $(= 1$ ms$)$ used in the data acquisition, whereas the time delay δt obtained by applying synchronization based on system identification can take any real number. This generally allows for more accurate synchronization.

Figure 6 shows the representation of the displacement and strain mode shapes obtained after compensation for the time delay $\delta t^\star$ in the complex plane. After minimization, some differences in MP remain $(f(3.6 \text{ ms}) \neq 0)$. This is also seen from table 2, which summarizes the results of the optimization. For modes 2, 3, and 4, the difference in MP value between the displacement and strain mode shape is significantly reduced. However, for mode 1, the difference in MP is not significantly reduced after the optimization. The remaining differences result from identification inaccuracies and violation of the assumptions in the proposed method. In the next section, it is shown that the estimated time delay $\delta t^\star$ is accurate, however, resulting in reliable estimates of the displacement and strain mode shapes.

When synchronization of more than two (n_acq) acquisition systems is needed, a reference system is chosen and the optimization procedure outlined in this section is repeated $n_\mathrm{acq} - 1$ times.

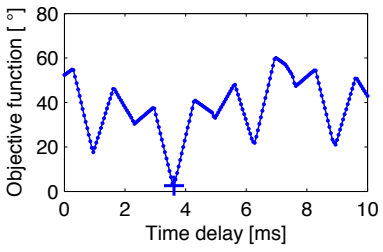

Figure 5: Variation of the objective function $f(\delta t)$ with the time delay δt. The marker (+) indicates the optimum.

Table 2: Summary of the optimization applied for the estimation of the time delay δt.

	mode 1	mode 2	mode 3	mode 4
$\mathrm{MP}(\boldsymbol{\phi}'_{\epsilon m}) - \mathrm{MP}(\boldsymbol{\phi}_{am})$	-7.64	-87.80	-63.29	50.70
$\mathrm{MP}(\boldsymbol{\phi}'_{\epsilon m} e^{\lambda_{m1}\delta t^\star}) - \mathrm{MP}(\boldsymbol{\phi}_{am})$	6.51	0.38	3.50	-0.01
$\theta^\star_m$	-14.15	-88.18	-246.79	-489.29
			$(= -66.79 - 180)$	$(= 50.71 - 540)$
$A^\star_m$	0.99	1.00	0.99	0.99

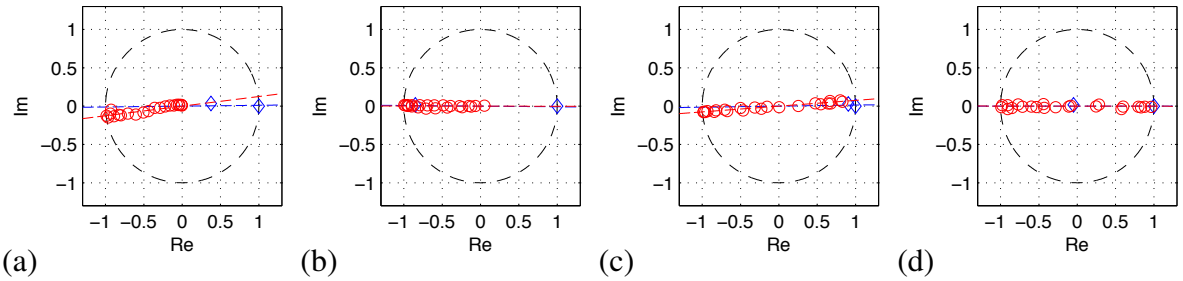

(a) (b) (c) (d)

Figure 6: Displacement (blue diamonds) and strain (red circles) mode shape components obtained after compensation for the time delay $\delta t^\star$ for (a) mode 1, (b) mode 2, (c) mode 3, and (d) mode 4, in the complex plane. A line fit for the displacement and strain mode shape is shown by a blue and red dashed line, respectively.

3.3 Verification

A verification experiment was performed. A vertical impact force was applied at the tip of the beam using the instrumented hammer (Fig. 3). The response of the beam was measured in all sensors. Fig. 7 shows a detail of the force time history, and the time history of the response obtained from accelerometer a_1 and strain gauge ϵ_5, that physically coincide. The force and acceleration signal have been acquired by the NI system, the strain signal by the FBGS system. A significant increase of the acceleration level is observed right after the impact is applied (Fig. 7b). The strain signal remains very small the first 4 ms after the impact, thereafter showing a significant decrease. The observed delay of $4\ \mathrm{ms} \pm 0.5\ \mathrm{ms}$ is in line with the delay δt of 3.62 ms that has been identified in Section 3.2.

Fig. 8 finally shows the displacement and strain mode shapes along the beam after accounting for the phase shift and amplitude modification introduced by the synchronization error. Only the real part of the mode shapes is retained. Due to the limited number of accelerometers, a proper distinction between the displacement mode shapes for different modes cannot be made. The strain mode shapes have a regular shape. The apparent deviation of the mode shape at sensor ϵ_3 is due to the presence of a bolt that is welded at the lower side of the beam to connect the shaker (see Fig. 2c). This results in (locally) lower strain levels.

4 CONCLUSIONS

It is shown in this paper that for linear structures with proportional damping a time lag between measured response signals results in a spurious phase shift of the corresponding mode shape components, whereas the natural frequencies and damping characteristics are unchanged. This observation can be used for (offline) synchronization of data acquisition systems, using the modal characteristics obtained from a system identification. The time lag is estimated from the solution of an optimization problem. A demonstration for a laboratory experiment on a cantilever steel beam has shown that the proposed methodology can be used for accurate time synchronization, with significant improvement of the accuracy of the identified mode shapes.

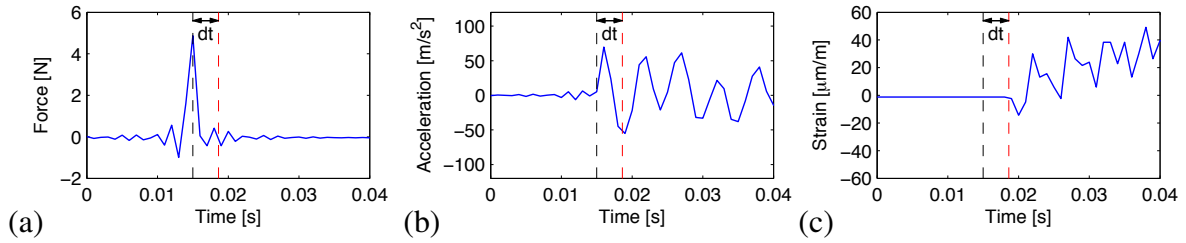

Figure 7: Time history of (a) the hammer impact and time history of the corresponding acceleration a_1 (b) and strain ϵ_1 (c). The time step corresponding to the peak force is indicated by a dashed black line. The time delay δt (=3.6 ms) is found as the horizontal distance between the dashed black line and the dashed red line.

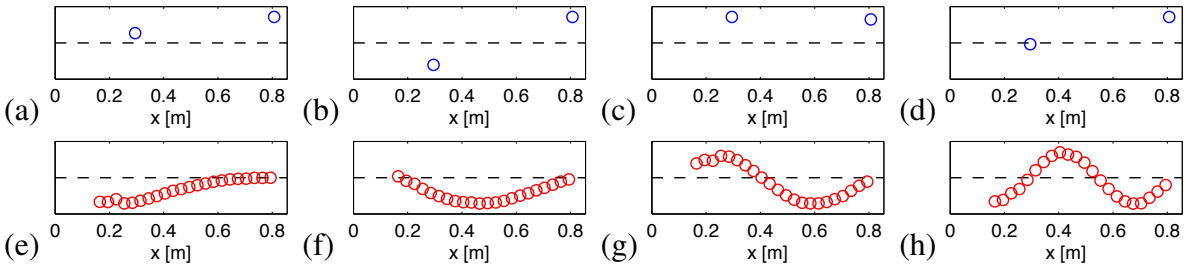

Figure 8: Displacement mode shapes (top, a – d) and strain mode shapes (bottom, e – h) along the axis of the beam, for mode 1 (a and e), mode 2 (b and f), mode 3 (c and g), and mode 4 (d and h).

ACKNOWLEDGEMENTS

The research presented in this paper has been performed within the framework of the project G.0738.11 “Inverse identification of wind loads on structures”, funded by the Research Foundation Flanders (FWO), Belgium. Kristof Maes is a Postdoctoral Fellow of KU Leuven. The financial support of FWO and KU Leuven is gratefully acknowledged. The authors affiliated to KU Leuven are all members of the KU Leuven - BOF PFV/10/002 OPTEC - Optimization in Engineering Center.

REFERENCES

[1] S. Amador, F. Magalhães, N. Martins, E. Caetano, and Á. Cunha. High spatial resolution operational modal analysis of a football stadium suspension roof. In Á. Cunha, L.F. Ramos, E. Caetano, and P. Lourenço, editors, *Proceedings of the 5th International Operational Modal Analysis Conference, IOMAC 2013*, Guimarães, Portugal, May 2013.

[2] A. Araujo, J. Garcia-Palacios, J. Blesa, F. Tirado, E. Romero, A. Samartin, and O. Nieto-Taladriz. Wireless measurement system for structural health monitoring with high time-synchronization accuracy. *IEEE Transactions on Instrumentation and Measurement*, 61(3):801–810, 2012.

[3] G.H. Golub and C.F. Van Loan. *Matrix computations*. John Hopkins University Press, Baltimore, MD, 3rd edition, 1996.

[4] W. Heylen, S. Lammens, and P. Sas. *Modal analysis theory and testing*. Department of Mechanical Engineering, Katholieke Universiteit Leuven, Leuven, Belgium, 1997.

[5] R. Kim, T. Nagayama, H. Jo, and B.F. Spencer Jr. Preliminary study of low-cost GPS receivers for time synchronization of wireless sensor networks. In *Proceedings of SPIE,*

Sensors and Smart Structures Technologies for Civil, Mechanical, and Aerospace Systems 2012, volume 8345, pages 83451A–1, 2012.

[6] E. Reynders. System identification methods for (operational) modal analysis: review and comparison. *Archives of Computational Methods in Engineering*, 19(1):51–124, 2012.

[7] E. Reynders and G. De Roeck. Reference-based combined deterministic-stochastic subspace identification for experimental and operational modal analysis. *Mechanical Systems and Signal Processing*, 22(3):617–637, 2008.

[8] E. Reynders, J. Houbrechts, and G. De Roeck. Fully automated (operational) modal analysis. *Mechanical Systems and Signal Processing*, 29:228–250, 2012.

[9] S. Van Huffel and J. Vandewalle. *The total least squares problem*. SIAM, Philadelphia, PA, 1991.

[10] M.L. Wang, J.P. Lynch, and H. Sohn, editors. *Sensor Technologies for Civil Infrastructures: Sensing Hardware and Data Collection Methods for Performance Assessment.*, volume 1. Elsevier, 2014.

[11] W. Weijtjens, G. De Sitter, C. Devriendt, and P. Guillaume. Operational modal parameter estimation of MIMO systems using transmissibility functions. *Automatica*, 50(2):559 – 564, 2014.

[12] D.V. Widder. *The Laplace Transform*. Princeton University Press, Princeton, 1946.